New Journal of Physics
The open–access journal for physics

Demonstration of frequency encoding in neutral atom lithography

J H Thywissen[1] **and M Prentiss**[2]

[1] Department of Physics, University of Toronto, 60 Saint George St, Toronto, Ontario M5S 1A7, Canada
[2] Department of Physics, Harvard University, Cambridge, MA 02138, USA

New Journal of Physics **7** (2005) 47
Received 14 July 2004
Published 9 February 2005
Online at http://www.njp.org/
doi:10.1088/1367-2630/7/1/047

Abstract. We demonstrate a frequency encoding technique for feature placement in atom lithography. Frequency encoding is widely used in MRI, where the frequency distribution of radio waves reveals the position distribution of nuclei in a magnetic gradient. Applied to neutral atom lithography, frequency encoding enables continuously adjustable feature positions and feature densities not limited by the optical wavelength, unlike intensity- or polarization-based patterning. Lines as narrow as $0.9 \pm 0.1\ \mu$m are fabricated on silicon and gold substrates when exposed to a metastable argon beam through two mask configurations of up to six laser beams.

PII: S1367-2630(05)83362-2

Contents

1. Introduction

Neutral atom beams patterned with masks of laser light are uniquely well-suited for structured doping [1, 2] and for fabrication demanding long-range coherent registration [3, 4]. Atom lithography has so far been able to make lines as small as 13 nm [5, 6], to fabricate features with aspect ratios greater than 2 : 1 [7, 8], and to pattern areas as large as 38 cm^2 [9, 10]. However, feature spacings in light masks have been limited by the length scale of the optical wavelength used [11]–[21]. In this work, we demonstrate a technique that could be used to extend light masks to more complex patterns than standing wave interferences and to features more closely spaced than the optical wavelength.

Research in neutral atom lithography has been motivated by several considerations. Neutral atomic beams need only low kinetic energies (50 meV) to have short (<0.1 nm) de Broglie wavelengths, minimizing diffractive resolution limitations. Compared to electrons and ions, neutral atoms are insensitive to stray electric and magnetic fields, and long-range inter-particle interactions are weak. Previous work has included the development of a wealth of atom optics (mirrors, guides, etc), including light masks which, unlike physical masks, do not sag and cannot be clogged or damaged. Laser-accessible internal structure of atoms allows efficient cooling, the storage of internal energy, and complex manipulations. State-sensitive atom lithography with metastable atoms has been demonstrated with both positive- and negative-tone resists capable of sub-10-nm resolution [22, 9, 23]. Though atom lithography has relatively long exposure times, patterning is a parallel process, and recent work has demonstrated a tenfold acceleration possible with chemical amplification [24].

In this work, we address the difficulty of previous schemes to create arbitrary patterns. We propose the encoding of the desired position distribution using the *frequency*, instead

of the intensity, of a laser beam.[3] In the presence of an appropriate field gradient, the resonant optical frequency of the atom can be position-dependent. Thus each spectral component of a probe laser beam can interact with the atoms at a specific but separate location. The frequency encoding of spatial information is commonly known from MRI, where protons (instead of atoms) are imaged (instead of patterned) in a potential gradient by radio- (instead of optical-) frequency radiation. We will refer to atom lithography with frequency-encoded light masks as atomic resonance lithography (ARL). Previous work by Thomas *et al* has developed neutral atom measurement techniques based on an analogue to nuclear magnetic resonance techniques [25, 26].

Just as sub-100-μm features can be resolved with 100 m wavelength radio waves in MRI, far sub-optical (i.e., sub-micron) features and spacings can be created with ARL [25]–[27]. As shown in [27], arbitrary one-dimensional patterns can be frequency-encoded and generated. Furthermore, ARL can create two-dimensional patterns, just as MRI can image two- [28] or three-dimensional distributions: by superposing a sequence of one-dimensional distributions. Finally, frequency-encoded masks do not demand high transverse coherence of the incident atoms.

In the following sections, we present two masking configurations. The first (section 2) is a simple, single-step process, which we use to demonstrate the flexibility of patterning. After discussion of the resolution of ARL (section 3), we use a more complicated process to pattern 0.9-μm features (section 4). We discuss our results and compare to atom holography, which can also create arbitrary patterns [29]–[31]. Finally, we discuss extensions of the demonstrated lithographic technique (section 5).

2. First experiment: multiple features on a single intensity gradient

2.1. Single-step optical mask

Figure 1 describes a realization of ARL based on quenching directly within the potential gradient. Firstly, metastable argon atoms are optically pumped to the $|J = 2, m_J = 2\rangle$ sublevel of the $4s[3/2]_2^o$ or $1s_5$ state.[4] Next, the atoms pass through a zone of two overlapping beams: a resonant σ^+ 'shift' beam (**S**) on the 812 nm $|J = 2, m_J = 2\rangle \rightarrow |J' = 3, m_{J'} = 3\rangle$ cycling transition overlaps with a σ^- 'quench' beam (**Q**) containing four frequency components, $\pm\delta_1$ and $\pm\delta_2$. As shown in figure 2(a), these frequencies are resonant at two Stark shifts (i.e., four positions) in the resonant shift beam. At these four positions, atoms are optically pumped by **Q** to the true atomic ground state $|g\rangle$, 'quenching' the internal energy. Note that two frequencies (e.g., $\pm\delta_1$) were required for complete optical pumping at each resonant position because atomic population exists in both the strong- and weak-field-seeking dressed states in the resonant **S** field. Thus, the detunings δ_1 and δ_2 control where quenching occurs.

[3] In this demonstration we do, in fact, use a light beam with an intensity gradient, in addition to the probe laser. However, no information about the pattern is contained in this gradient, i.e., the same gradient could be used for different patterns. More generally, the 'field gradient' mentioned above can be a gradient in a magnetic, electrostatic, or light field.

[4] A second metastable state of argon, $4s'[1/2]_0^o$ or $1s_3$, is also produced by our source, but we eliminate those atoms with an earlier optical quenching stage. If unquenched, these '$J = 0$' atoms would contribute a background rate of resistance formation.

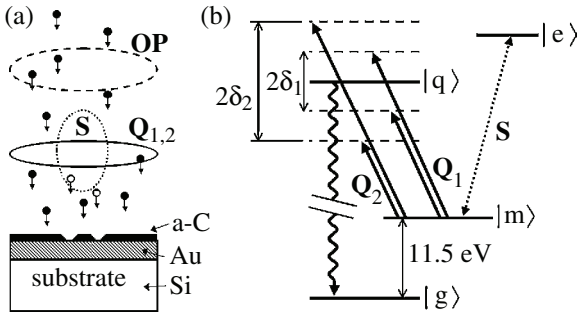

Figure 1. The single-step light mask used for atomic resonance lithography. (a) Argon atoms strike a gold surface after passing through a sequence of laser beams (cross-sections shown as ovals, not to scale) propagating out-of-plane and parallel to the substrate surface: optical pump **OP**, Stark shift **S**, and quench **Q**. The light mask selectively quenches some atoms to their ground state $|g\rangle$ ($\circ$), in which state atoms are unable to activate the formation of resist on the surface. At all other locations, metastable atoms $|m\rangle$ ($\bullet$) activate the growth of carbonaceous resist (a-C) on the substrate. (b) Level diagram relevant to **S** and **Q**. An on-resonant light shift beam (**S**) is applied on a cycling transition between the metastable state $|m\rangle$ and excited state $|e\rangle$. The quench lasers $\mathbf{Q}_1$ and $\mathbf{Q}_2$, detuned $\pm\delta_1$ and $\pm\delta_2$, respectively, optically pump atoms to the ground state $|g\rangle$ via the excited state $|q\rangle$ and a radiative cascade.

The mechanism by which internal state manipulation creates a lithographic pattern has been discussed elsewhere [8, 9, 24]. Briefly, the process exploits the internal energy difference between the ground state and the $4s[3/2]_2^o$ metastable state of argon: atoms in $|m\rangle$ release 11.5 eV of internal energy to activate the formation of a resist on the surface, while atoms in $|g\rangle$ do not affect the surface. The resist material is not formed out of argon, but instead from physisorbed hydrocarbons released from the diffusion pumps that evacuate the vacuum chamber. Exposure to metastable atoms induces a chemical change that results in the formation of a durable material. This resist material remains on the surface even after exposure to air and/or solution, and can thus be used as a mask for etching.

2.2. Experiment and results

A metastable argon (Ar*) beam with a flux density of $3 \times 10^{12}\,\mathrm{cm}^{-2}\,\mathrm{s}^{-1}$ is incident on a gold substrate for 5 h with the optical configuration of figure 1. The light mask parameters are as follows: The 5.9 mW **S** beam is cylindrically focused to a profile of 46 μm $\times$925 μm, creating a maximum Stark shift that was spectroscopically measured to be 150 MHz. Cylindrically symmetric 110 μm-wide quench beams $\mathbf{Q}_1$ and $\mathbf{Q}_2$ each having 70 μW of power, split between the pair of detunings, $\pm\delta_1 = \pm 2\pi \times 40$ MHz and $\pm\delta_2 = \pm 2\pi \times 110$ MHz. After exposure, the substrate is removed from the vacuum system and etched for 7 min in a ferricyanide solution.

Figure 2 shows the correspondence between the light mask configuration and the pattern observed on the etched substrate. At positions where either $\mathbf{Q}_1$ or $\mathbf{Q}_2$ was resonant, metastable atoms are quenched, leaving the underlying substrate unprotected against the subsequent gold etch. At all other positions, a resist material is formed, and gold remains on the silicon substrate

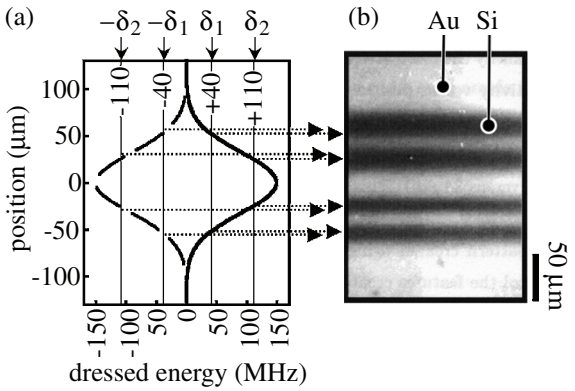

Figure 2. (a) Energy times $1/h$ (horizontal axis) versus position (vertical axis) of the weak (——) and strong (– – –) field-seeking dressed states of an atom in the **S** beam. Thin vertical solid lines show the resonaces when the dressed energy is equal to the quench laser detunings: at $E/h = \pm\delta_1$ and $E/h = \pm\delta_2$. (b) Optical micrograph of a gold-on-silicon substrate after exposure and etch. The dark lines are exposed silicon, and correspond to locations where atoms were quenched, thus preventing the formation of a resist and allowing gold to be etched. These features are formed at resonant quench locations, as indicated by dotted arrows between (a) and (b).

after etching. A pattern was formed across 2 cm of the substrate. Figure 2(b) was taken in the centre of that pattern, where atoms entered perpendicular to the light mask. We fit the sum of four Lorentzians to the integrated reflectivity profile of the substrate to determine the feature widths and positions. The lower (upper) two lines have a half-width of 10 ± 1 μm (14 ± 1 μm) and a centre-to-centre separation of 26 ± 2 μm (34 ± 2 μm). The asymmetry between the upper and lower set could be explained by aberrations in the cylindrical optics that formed the shift beam. The lower set of lines are within experimental error of the expected line width, 9 μm (as discussed below), and the expected feature separation, 27 μm.[5]

3. Discussion: resolution limitations in ARL

The significance of the result shown in figure 2 is that two lithographic features were created across each monotonic part of the potential. Unlike previous atom lithographic results with light masks, *the wavelength of light does not determine the minimum feature separation.* Nor are complex potentials necessary for a complex pattern. The ultimate resolution of ARL can be limited by a variety of effects, discussed by Thomas [25] and Olshanii [27], and summarized in the following paragraphs. Note that although in microscopy the resolution is defined as the minimum distinguishable feature spacing, in this and many other lithography experiments, feature size is the only indication of resolution.

[5] Note that the transfer function from atomic flux density to reflectivity of the surface after etching is nonlinear, such that purely atomic calculations of feature width may vary systematically from the observed features.

3.1. Spectroscopic limit

The most fundamental limitation is the spectroscopic precision with which each resonant transfer position is defined,

$$\delta x_{\mathrm{sp}} = \frac{\hbar \Gamma'}{F}, \tag{1}$$

where Γ' is the spectroscopic width of the transition, and F is the potential gradient. In these experiments we used laser light to create the potential gradient, but gradients could also be created with magnetic [26] or electric fields. For the realization of ARL discussed above, Γ' is the power-broadened and time-broadened quenching transition, with a natural line width $\Gamma = 2\pi \times 5.83\,\mathrm{MHz}$. Experimentally, we measure $\Gamma' = 2\pi \times 20 \pm 2\,\mathrm{MHz}$. For the gradient $F/\hbar = 2\pi \times 2.3\,\mathrm{MHz}\,\mu\mathrm{m}^{-1}$ at the feature locations in figure 2, we find $\delta x_{\mathrm{sp}} = 9\,\mu\mathrm{m}$. Note that for a Raman transition, as will be considered below, $\Gamma' = v_L/w_0 = 1/\tau$, where $v_L = 850 \pm 40\,\mathrm{m\,s}^{-1}$ is the mean longitudinal velocity of the Ar* atoms, w_0 is the $1/e^2$ intensity waist of the Raman beams, and τ is the atom–light interaction time.

3.2. Acceleration and diffraction

Atomic motion during the transfer can also limit the resolution. While transferring an atom of mass M to a state with a gradient F, acceleration and diffraction limit the resolution to the order of $F\tau^2/2M$, where τ is again the transfer time [25]. However, the numerical factors depend on which states are in a gradient and for how long. In the case where Γ' is determined by the interaction time of a Raman transfer, and the pattern is formed by the atoms transferred to the gradient, one can choose an optimal τ to give a resolution of

$$\delta x_{\ell} = 2(\hbar^2/2MF)^{1/3}. \tag{2}$$

For ^{40}Ar and $F/\hbar = 2\pi \times 1\,\mathrm{MHz}\,\mu\mathrm{m}^{-1}$, the optimal size is $\delta x_{\ell} = 100\,\mathrm{nm}$. This limit is not, however, fundamental: Olshanii *et al* show that an appropriate choice of probe frequency variation during atomic transfer (a 'magic phase') can correct for later evolution, such that the spectroscopic resolution δx_{sp} is recovered [27].

Free flight between the pattern formation and the substrate will allow the atoms to diffract further. Given a free-flight time T_{FF}, the diffraction limit is

$$\delta x_{\mathrm{dif}} = \sqrt{\hbar T_{FF}/2M}. \tag{3}$$

For instance, for $T_{FF} = 30\Gamma^{-1}$, this limit is $\delta x_{\mathrm{dif}} = 27\,\mathrm{nm}$, smaller than the other limits given here. Note that this is a quantitative restatement of one of the desirable qualities of atoms as a patterning constituent: their short de Broglie wavelength λ_{dB} minimizes the diffraction, $\sim\sqrt{\lambda_{dB} D}$, where D is the mask–substrate separation.

3.3. Transverse coherence

Finally, the collimation of the atomic beam poses a limit on the observable resolution. Given an rms velocity spread v_{rms}, the resolution is limited to

$$\delta x_{\mathrm{v}} \approx v_{rms}(\tau + T_{FF}). \tag{4}$$

Typical parameters for our experiment are $\tau + T_{FF} = 30\Gamma^{-1}$, and $v_{\mathrm{rms}} = 0.5\,\mathrm{m\,s}^{-1}$, and thus features cannot be smaller than $\delta x_{\mathrm{v}} = 0.4\,\mu\mathrm{m}$ wide.

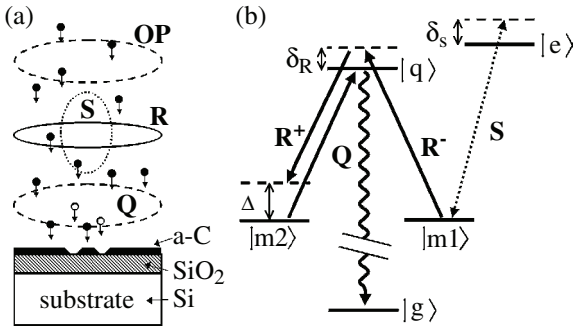

Figure 3. ARL light mask using two-photon transfer and dark states. (a) The geometrical arrangement of the light mask. Argon atoms strike a gold surface after passing through a sequence of laser beams (cross-sections shown as ovals, not to scale) propagating out-of-plane and parallel to the substrate surface. The substrate consists of a 15 nm silicon-dioxide layer over a bulk silicon layer. A uniform magnetic field, not shown, is parallel to the laser beams. (b) Atoms are prepared in the state $|\mathrm{m1}\rangle$ optical pump transition (not shown). At locations where the Stark shift of the **S** beam matches the differential detuning Δ of the Raman beams ($\mathbf{R}^+$ and $\mathbf{R}^-$), atoms are transfered to $|\mathrm{m2}\rangle$. In the subsequent quenching zone, atoms in $|\mathrm{m2}\rangle$ are optically pumped to $|\mathrm{g}\rangle$ by **Q**.

4. Second experiment: sub-micron features

In order to improve our resolution, we performed a second experiment with several experimental modifications. Firstly, we improved the quality of the optics forming the **S** beam to reduce the waist by a factor of 3. Next, as shown in figure 3, we used a coherent transfer scheme by detuning the **S** beam by 2.0 GHz and introducing Raman beams. At resonant positions in the light mask, the Raman beams transfer atoms from $|\mathrm{m1}\rangle$ to $|\mathrm{m2}\rangle$. In the third interaction zone, only the atoms transferred to $|\mathrm{m2}\rangle$ are quenched.[6] With such a scheme, we realized a factor of 10 improvement in resolution, as described below. Furthermore, such a coherent ARL scheme avoids momentum diffusion by spontaneous emission, and can implement further resolution improvements such as the coherent manipulations described in [27].

4.1. Two-step light mask

A silicon $\langle 100\rangle$ substrate with a 15 nm oxide layer was exposed for 6 h through the ARL mask depicted in figure 3. The **R** beam of 25 μm by 103 μm has σ^- and σ^+ components with powers of 65 and 60 μW and detunings of +61.1 and +104.2 MHz, respectively. A 1.3 G quantization field reduces the differential detuning by 5.4 MHz, such that the net Raman detuning is $\Delta/2\pi = -37.7$ MHz. The shift beam **S** has 6.9 ± 0.3 mW of power and a profile of $15 \pm 1\ \mu\mathrm{m} \times 250\ \mu\mathrm{m}$, and is tuned $\delta_S/2\pi = 2.00$ GHz above resonance. The σ^+ polarized **S** beam interacts with both $|\mathrm{m1}\rangle$ and $|\mathrm{m2}\rangle$, but gives a differential gradient $F/\hbar = 2\pi \times 6.4$ MHz $\mu\mathrm{m}^{-1}$ due to the difference in Clebsh–Gordan coefficients: 1 and $\sqrt{2/5}$, respectively (note that figure 3 shows only the transition $|\mathrm{m1}\rangle - |\mathrm{e}\rangle$, for simplicity). The third interaction zone has a

[6] Whether to quench $|\mathrm{m1}\rangle$ or $|\mathrm{m2}\rangle$ depends on the tone of the resist and type of pattern desired.

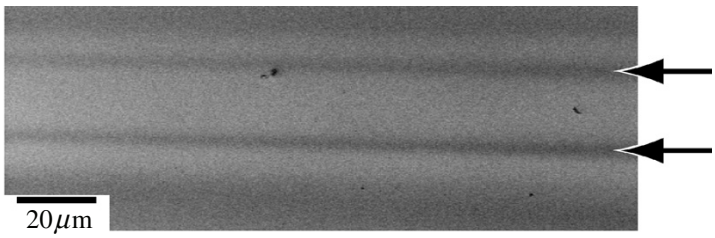

Figure 4. SEM image of a Si ⟨100⟩ substrate patterned by the light mask shown in figure 3. The darker lines (indicated by arrows) are places at which metastable atoms were quenched, thus preventing the formation of a resist material and allowing the silicon to be etched.

350 μW quench beam (**Q**) with a waist of 210 μm, such that about 12 photons are scattered from atoms in |m2⟩, sufficient to optically pump to |g⟩. Atoms that have been transferred to the |m2⟩ state are therefore quenched. Atoms in the |m1⟩ state are not quenched by the σ^+ polarized **Q** light, since they are in a dark state (|2, +2⟩). The latter atoms arrive at the substrate in the metastable state and can therefore activate resist formation.

After exposure, the pattern was transferred to the substrate using both dry and wet etches. Firstly, the sample was etched for 35 s in a CHF_3 reactive ion etch with parameters 42 mTorr chamber pressure, 100 W forward power, 10 W reflected power, −842 V self-bias, and 25.0 sccm flow rate. Secondly, the sample was etched for 50 s in 2% HF to prepare an unoxidized silicon face. Finally, the sample was etched for 14 min in 20% KOH at 22 °C [8].

4.2. Results and discussion

Figure 4 shows a scanning electron micrograph of the etched sample. The features created by ARL are indicated by arrows. Two features are created with a single Raman detuning because the Stark shift is equal to Δ at a location to either side of its maximum. The dark lines against a bright background indicate places at which silicon was preferentially etched. The sample was patterned across several millimetres of length. At the centre, for the run parameters above (gradient $F/\hbar = 2\pi \times 6.4 \pm 0.5\,\mathrm{MHz}\,\mu\mathrm{m}^{-1}$ and $\tau = 29 \pm 2$ ns), the expected feature separation is $19.0 \pm 1.5\,\mu$m, and the spectroscopic limit is $\delta x_{\mathrm{sp}} = 0.86 \pm 0.07\,\mu$m. This agrees well with our measurements: a minimum spacing of $(20.0 \pm 0.4)\,\mu$m and an rms width of $(0.9 \pm 0.1)\,\mu$m.

It is interesting to compare these results with the features detected in holographic masking experiments for neutral atoms [29]–[31]. Holographic techniques have created intricate, two-dimensional patterns, which are detected by a microchannel plate. The demonstrated resolution was 65 μm, though in principle feature size is only limited by the holes in the hologram, which can be less than 100 nm across. By comparison, our technique is a type of contact printing, where diffraction is avoided due to the small de Broglie wavelength of massive particles. Unlike holography, spatial coherence is not required across the entire mask: in fact, with a velocity spread of 0.5 m s^{-1}, we have a transverse coherence of only 20 nm, for a mask over 10 μm wide. Higher coherence length sources are only available at much lower flux, and thus the patterns observed in [29]–[31] were formed with less than 10^6 atoms across areas of approximately 1 mm^2, insufficient to pattern a substrate—which typically requires over 10^{15} atoms cm^{-2}. Thus, atom holography has not yet been used for lithography. In contrast, the patterns in figures 2 and 4 were

formed after an exposure of approximately 5×10^{16} atoms cm^{-2}, sufficient to pattern gold and silicon substrates.

Although μm-scale, the features shown here are still two orders of magnitude larger than the smallest features fabricated with neutral atom lithography [5]–[8]. If the light gradient were to be increased, feature sizes in the second ARL scheme demonstrated would be limited by the velocity spread of the atomic beam, at $\delta x_{\mathrm{v}} = 0.4\,\mu$m. Therefore, the spectroscopically limited feature size observed in figure 4 is a factor of two above the minimum observable linewidth for the collimation of our atomic beam. By comparison, the resolution limit of an optimized light mask with a gradient of $F/\hbar = 2\pi \times 6.4\,\mathrm{MHz}\,\mu\mathrm{m}^{-1}$ is $\delta x_{\ell} = 54\,\mathrm{nm}$ for Ar*.

5. Conclusions and prospects

In conclusion, we have demonstrated the use of frequency encoding in optical masks for atom lithography. Using a two-photon internal state transfer, we create features in silicon with an rms width of $0.9 \pm 0.1\,\mu$m. With a mask based on optical pumping, we show that feature position can be chosen continuously throughout monotonic potential gradients.

The potential gradients we have used here were created by near-resonant laser light. However potentials could also be created using a magnetic field, which could be made uniform across a larger area. A magnetic gradient B' would give a differential potential energy gradient $F = \mu_{\mathrm{B}} g B'$, where μ_{B} is the Bohr magneton and g is the Landé g-factor. For example, the states we have been considering in argon have $g \approx 1.5$, such that a gradient of $500\,\mathrm{G\,cm}^{-1}$ would give $F/\hbar = 2\pi \times 0.1\,\mathrm{MHz}\,\mu\mathrm{m}^{-1}$. Although this gradient is lower than those used in the above experiments, using a magnetic field might be advantageous for a longer interaction time, or a larger patterned area.

We have demonstrated very simple one-dimensional patterning with a single expsoure, but as discussed in [27], arbitrary patterns can be produced up to the resolution limit of the technique. Furthermore, this technique can be extended to two-dimensional patterning with multiple exposures. This extension is similar to medical imaging with MRI, in which the potential gradient is rotated during imaging. As discussed in [28], a series of one-dimensional projections can define a two-dimensional pattern. The requirement of a series of depositions would increase the required exposure time, but not as quickly as would be required for serial writing of a two-dimensional pattern: a pattern with N pixels requires writing time that scales as $\sqrt{N}$, essentially because the writing process remains a parallel process for a one-dimensional set of pixels. Thus, ARL can be used to form intricate, sub-micron, two-dimensional patterns.

A practical issue for the experiments shown here is the exposure time. Although 5 h exposure times are acceptable for research purposes, lengthier exposures—for instance for more complex patterns—may be impractical. Recent work [24] has shown that doses as small as 3×10^{14} atoms cm^{-2} are sufficient to damage self-assembled monolayers, which has been shown to be a resist for neutral atoms [22]. Thus, it may be possible to reduce the exposure time by two orders of magnitude by improving the resist used. Another approach to reducing exposure time would be to use an alkali metal source, which can be much brighter than a metastable noble gas source. Lithography using ARL and similar internal-manipulation schemes could also be extended to alkali atoms by state-selective ionization and deflection. Neutral alkali atoms, like unquenched metastable atoms, would be left to pattern an atom resist (e.g. [32]).

Acknowledgments

The authors thank N Dekker and K S Johnson for contributions to the early stages of this project. We also thank F Altarelli, G Zabow and S Coutreau for assistance.

References

[1] Schulze Th, Müther T, Jürgens D, Brezger B, Oberthaler M K, Pfau T and Mlynek J 2001 *Appl. Phys. Lett.* **78** 1781
[2] Oberthaler M K and Pfau T 2003 *J. Phys.: Condens. Matter* **15** R233
[3] Thywissen J H, Johnson K S, Dekker N H, Chu A P and Prentiss M 1998 *J. Vac. Sci. Technol.* B **16** 3841
[4] McClelland J J, Anderson W R, Bradley C C, Walkiewicz M, Celotta R J, Jurdik E and Deslattes R D 2003 *J. Res. NIST* **108** 99
[5] Behringer R E, Natarajan V, Timp G and Tennant D M 1996 *J. Vac. Sci. Technol.* B **14** 4072
[6] Anderson W R, Bradley C C, McClelland J J and Celotta R J 1999 *Phys. Rev.* A **59** 2476
[7] Rehse S J, Glueck A D, Lee S A, Goulakov A B, Menoni C S, Ralph D C, Johnson K S and Prentiss M 1997 *Appl. Phys. Lett.* **71** 1427
[8] Thywissen J H, Johnson K S, Dekker N H, Prentiss M, Wong S S, Weiss M and Grunze M 1998 *J. Vac. Sci. Technol.* B **16** 1155
[9] Johnson K S *et al* 1996 *Appl. Phys. Lett.* **69** 2773
[10] For a review of neutral atom lithography, see Meschede D and Metcalf H 2003 *J. Phys. D: Appl. Phys.* **36** R17
[11] Timp G, Behringer R E, Tennant D M, Cunningham J E, Prentiss M and Berggren K K 1992 *Phys. Rev. Lett.* **69** 1636
[12] McClelland J J, Scholten R E, Palm E C and Celotta R J 1993 *Science* **262** 877
[13] McGowan R W, Giltner D M and Lee S A 1995 *Opt. Lett.* **20** 2535
[14] Gupta R, McClelland J J, Jabbour Z J and Celotta R J 1995 *Appl. Phys. Lett.* **67** 1378
Drodofsky U, Stuhler J, Schulze T, Drewsen M, Brezger B, Pfau T and Mlynek J 1997 *Appl. Phys.* B **65** 755
[15] Features spaced by $\lambda/8$ were created in Gupta R, McClelland J J, Celotta R J and Marte P 1996 *Phys. Rev. Lett.* **76** 4689
[16] Drodofsky U, Stuhler J, Brezger B, Schulze Th, Drewsen M, Pfau T and Mlynek J 1997 *Microelectron. Eng.* **35** 285
[17] Lison F, Adams H-J, Haubrich D, Kreis M, Nowak S and Meschede D 1997 *Appl. Phys.* B **65** 419
[18] Johnson K S, Thywissen J H, Dekker N H, Berggren K K, Chu A P, Younkin R and Prentiss M 1998 *Science* **280** 1583
[19] Engels P, Salewski S, Levsen H, Sengstock K and Ertmer W 1999 *Appl. Phys.* B **69** 407
[20] Brezger B, Schulze Th, Schmidt P O, Mertens R, Pfau T and Mlynek J 1999 *Europhys. Lett.* **46** 148
[21] Mützel M, Tandler S, Haubrich D, Meschede D, Peithmann K, Flasphler M and Buse K 2002 *Phys. Rev. Lett.* **88** 083601
[22] Berggren K K, Bard A, Wilbur J L, Gillaspy J D, Helg A G, McClelland J J, Rolston S L, Phillips W D, Prentiss M and Whitesides G M 1995 *Science* **269** 1255
[23] Hill S B, Haich C A, Dunning F B, Walters G K, McClelland J J, Celotta R J and Craighead H G 1999 *Appl. Phys. Lett.* **74** 2239
[24] Chabinyc M, Love C, Thywissen J H, Cervelli F, Prentiss M and Whitesides G M 2003 *Langmuir* **19** 2201
[25] Thomas J E 1989 *Opt. Lett.* **14** 1186
Thomas J E 1990 *Phys. Rev.* A **42** 5652
Thomas J E and Wang L J 1995 *Phys. Rep.* **262** 311
[26] Stokes K D, Schnurr C, Gardner J R, Marable M, Welch G R and Thomas J E 1991 *Phys. Rev. Lett.* **67** 1997
Gardner J R, Marable M L, Welch G R and Thomas J E 1993 *Phys. Rev. Lett.* **70** 3404
[27] Olshanii M, Dekker N, Herzog C and Prentiss M 2000 *Phys. Rev.* A **62** 033612

[28] Lauterbur P C 1973 *Nature* **242** 190
[29] Fujita J, Morinaga M, Kishimoto T, Yasuda M, Matsui S and Shimizu F 1996 *Nature* **380** 691
[30] Morinaga M, Yasuda M, Kishimoto T and Shimizu F 1996 *Phys. Rev. Lett.* **77** 802
[31] Shimizu F 2000 *Adv. Atom. Mol. Opt. Phys.* **42** 73
[32] Kreis M, Lison F, Haubrich D, Meschede D, Nowak S, Pfau T and Mlynek J 1996 *Appl. Phys.* B **63** 649
Berggren K K, Younkin R, Cheung E, Prentiss M, Black A J, Whitesides G M, Ralph D C, Black C T and Tinkham M 1997 *Adv. Mater.* **9** 52